Supporting Information

Recycling spent $LiNi_{1-x-y}Mn_xCo_yO_2$ cathodes to bifunctional NiMnCo catalysts for zinc-air batteries

Miaolun Jiao, Qi Zhang, Chenliang Ye, Zhibo Liu, Xiongwei Zhong, Junxiong Wang, Chuang Li, Lixin Dai, Guangmin Zhou,* Hui-Ming Cheng*

Experimental Section

Electrocatalytic Measurements

Electrocatalytic performance of the catalysts was evaluated by linear sweep voltammetry (LSV) curves, which were conducted in a three-electrode system by a CHI 760E electrochemical workstation. A rotating disk electrode (RDE) coated with catalyst was used as the working electrode, Hg/HgO and graphite rode were served as reference and counter electrode, respectively. The catalyst ink was prepared with 2 mg active materials, 0.5 mg acetylene black, 25 μL 5 wt% Nafion solution, and 375 μL isopropanol/H_2O (v:v = 1:1) mixed solvent. 15 μL catalyst ink was dropped onto a disk electrode with the mass loading of 0.38 mg cm^{-2}. The oxygen reduction reaction (ORR) was measured in O_2-saturated 0.1 M KOH solution with the rotating speed varies from 400 rpm to 2025 rpm with the scan rage of 10 mV s^{-1}. The oxygen evolution reaction (OER) was measured in Ar_2-saturated 1 M KOH solution at the rotating speed of 1600 rpm with the scan rage of 10 mV s^{-1}. To monitor the production of H_2O_2 and calculate the electron transfer number, rotating ring-disk electrode (RRDE) measurement was carried out in O_2-saturated 0.1 M KOH and the ring potential was constant at 1.5 V vs. RHE. The electron transfer number (n) and peroxide yield (H_2O_2%) were calculated by the following equations:

$$n = 4 \times I_d / (I_d + I_r / N) \quad (1)$$

$$H_2O_2\% = 200 \times (I_r / N) / (I_d + I_r / N) \quad (2)$$

where I_d and I_r are disk current and ring current, respectively. N is the current collection efficiency (0.37) of the Pt ring.

Electrochemical performance of zinc-air batteries

The rechargeable zinc-air battery (ZAB) was assembled into a homemade device with the catalyst-based air cathode and zinc plate anode. The air cathode was prepared by mixing the catalyst, acetylene black, and 5 wt% Nafion solution with the mass ratio of 6:2:2 in isopropanol/H_2O (v:v = 1:1) solvent and casting the obtained homogenous slurry onto a carbon cloth with the mass loading of 1 mg cm^{-2}. The mixed solution of 6 M KOH and 0.2 M $ZnAc_2$ was used as the electrolyte of ZABs. The discharge performance and cycle performance of ZABs were tested on a Land CT2001 A battery test system. The polarization curve of ZAB was measured on a CHI 760E electrochemical workstation at the scan rate of 10 mV s^{-1}.

Flexible zinc-air battery was assembled with our catalyst cathode, zinc plate anode, and the PVA-KOH based gel-electrolyte. 5 g PVA124 powers was dissolved into 40 mL deionic water under violently stirring at 90 ℃, then 10 mL KOH solution (0.5 g mL^{-1}) was dropwise added into the PVA solution. After freezing the mixed solution in a refrigerator for three times, the PVA-KOH gel-electrolyte was obtained. During the assembly process of flexible ZABs, the PVA-KOH gel-electrolyte was sanwiched between the air cathode and zinc plate anode, and sealed by medical breathable tape and polyimide (PI) tape in the cathode side and anode side, respectively.

Density functional theory (DFT) calculation

All the computations were performed by means of spin-polarized density functional theory (DFT) methods with the PBE exchange correlation functional using the VASP code.[1] We take the DFT+U approach [2] to modify the intra-atomic Coulomb interaction among strongly correlated Co, Mn, and Ni 3d electrons. The DFT+U method used here is a simplified rotationally invariant formulation by Dudarev et al.,[3] where the on-site Coulomb parameter, U, and exchange parameter, J, are combined into a single parameter, $U_{eff} = U - J$. In the calculations, we applied U_{eff} = 5, 3.5,

4 eV for Ni, Co and Mn 3d electrons, respectively, which are optimized by the initial values from the literatures.[4] The van der Waals interactions were described using vdw-d3. A plane wave basis set with an energy cutoff of 400 eV was utilized to represent the valence electrons with a PAW representation of the core electrons. The self-consistent electron density was determined using iterative diagonalization of the Kohn–Sham Hamiltonian, with the occupation of the Kohn–Sham states being smeared according to a Fermi–Dirac distribution with a smearing parameter of k_{BT} = 0.1 eV. The Brillouin zone (periodic boundary conditions was sampled by 3 × 2 × 1 k-points with the Monkhorst–Pack scheme for all the surfaces.

We modeled the core-sell NiMnCo-AC with Ni(111) as the substrate and $NiMnCoO_4$(110) as the catalyst layer. The substrate and the bottom two layers of the $NiMnCoO_4$(110) were frozen and the uppermost layers as well as the adsorbed species were allowed to relax. Boundary conditions were periodic in the x and y directions and surfaces were separated by 15 Å of vacuum in the z direction. The structural optimization was considered converged when the forces on all moveable atoms were below 0.01 eV $Å^{-1}$ in any direction.

The adsorption energies (ΔE_{ad}) were calculated using the following formula:

$$\Delta E_{ad} = E_{surface+ad} - E_{surface} - E_{ad}$$

where $E_{surface+ad}$ is the energy of species adsorbed on the surface, $E_{surface}$ is the energy of the clean surface, and E_{ad} is the energy of the corresponding species in the gas phase.

The Gibbs free energy change (ΔG) of every elemental step was calculated using the computational hydrogen electrode (CHE) model proposed by Nørskov et al.,[5] which uses one-half of the chemical potential of hydrogen as the chemical potential of the proton−electron pair. Then, the ΔG value can be determined as follows:

$$\Delta G = \Delta E + \Delta ZPE - T\Delta S + \Delta G_U + \Delta G_{pH},$$

where ΔE is the electronic energy difference directly obtained from DFT calculations, ΔZPE is the change in zero-point energies, T is the temperature (T = 298.15 K), and ΔS is the entropy change. ΔG_U is the free energy contribution related to electrode potential U. ΔG_{pH} is the correction of the H^+ free energy by the concentration, which can be determined as $\Delta G_{pH} = 2.303 \times k_{BT} \times pH$ (or $0.059 \times pH$), where k_B is the Boltzmann constant. According to this equation, the free energies of each elementary step are increased with increasing pH values, while the overpotential is unchanged. The zero-point energies and entropies of the adsorption species were computed from the vibrational frequencies, in which only the adsorbate vibrational modes were calculated explicitly, while the catalyst sheet was fixed. The entropies and vibrational frequencies of molecules in the gas phase were taken from the NIST database.

References:

1. Kresse, G.; Furthmuller, J., Efficiency of Ab-initio Total Energy Calculations for Metals and Semiconductors Using a Plane-Wave Basis Set. *Computational Materials Science* **1996,** *6*, 15-50.
2. Anisimov, V. V.; Zaanen, J.; Andersen, O. K., Band theory and Mott insulators: Hubbard U instead of Stoner I. *Physical Review B* **1991,** *44* (3), 943-954.
3. Dudarev, S. L.; Botton, G. A.; Savrasov, S. Y.; Humphreys, C. J.; Sutton, A. P., Electron-Energy-Loss Spectra and the Structural Stability of Nickel Oxide: An LSDA+U Study. *Physical Review B* **1998,** *57* (3), 1505-1509.
4. Fu, Z.; Yang, B.; Zhang, Y.; Zhang, N.; Yang, Z., Dopant segregation and CO adsorption on doped Fe_3O_4 (1 1 1) surfaces: A first-principle study. *Journal of Catalysis* **2018,** *364*, 291-296.
5. Peterson, A. A.; Abild-Pedersen, F.; Studt, F.; Rossmeisl, J.; Nørskov, J. K., How copper catalyzes the electroreduction of carbon dioxide into hydrocarbon fuels. *Energy & Environmental Science* **2010,** *3* (9), 1311-1315.

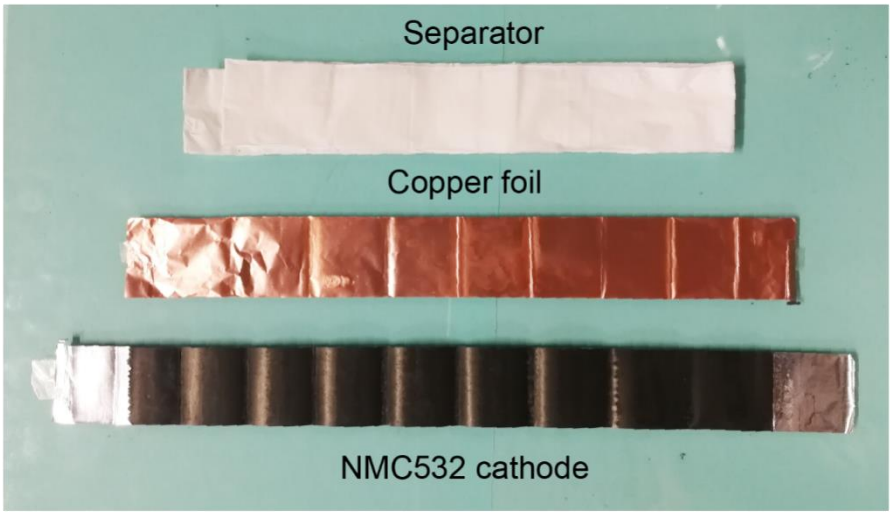

Figure S1 The separator, copper foil, and $LiNi_{0.5}Mn_{0.3}Co_{0.2}O_2$ (NMC532) cathode of the spent lithium-ion battery after disassembly. The graphite materials are peeled off from copper foil due to the Carboxymethyl cellulose (CMC) binder dissolved into water during the disassemble process. The NMC532 cathode are kept intact.

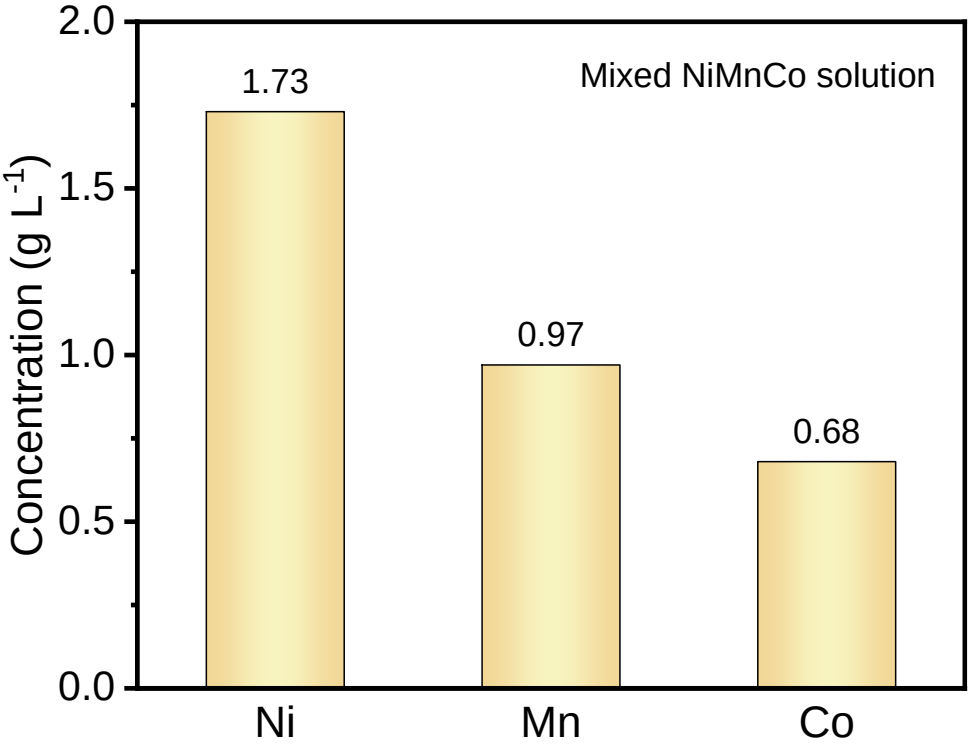

Figure S2 The concentrations of Ni, Mn, and Co in the mixed NiMnCo solution. 0.5 g recycled NMC532 powders are dissolved in nitric acid and diluted into 100 mL mixed NiMnCo solution, then the concentration of Ni, Mn, and Co were detected by inductively coupled plasma optical emission spectrometer (ICP-OES).

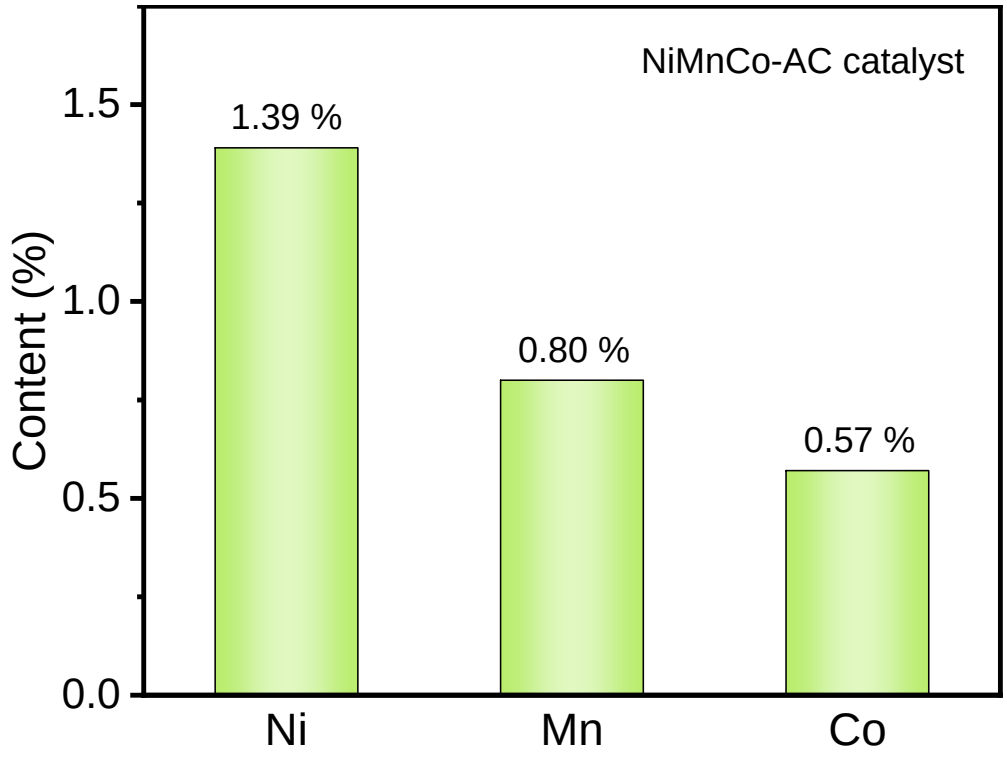

Figure S3 The contents of the Ni, Mn, and Co in the prepared NiMnCo-AC catalyst, which was tested by ICP-OES after the acid digestion process.

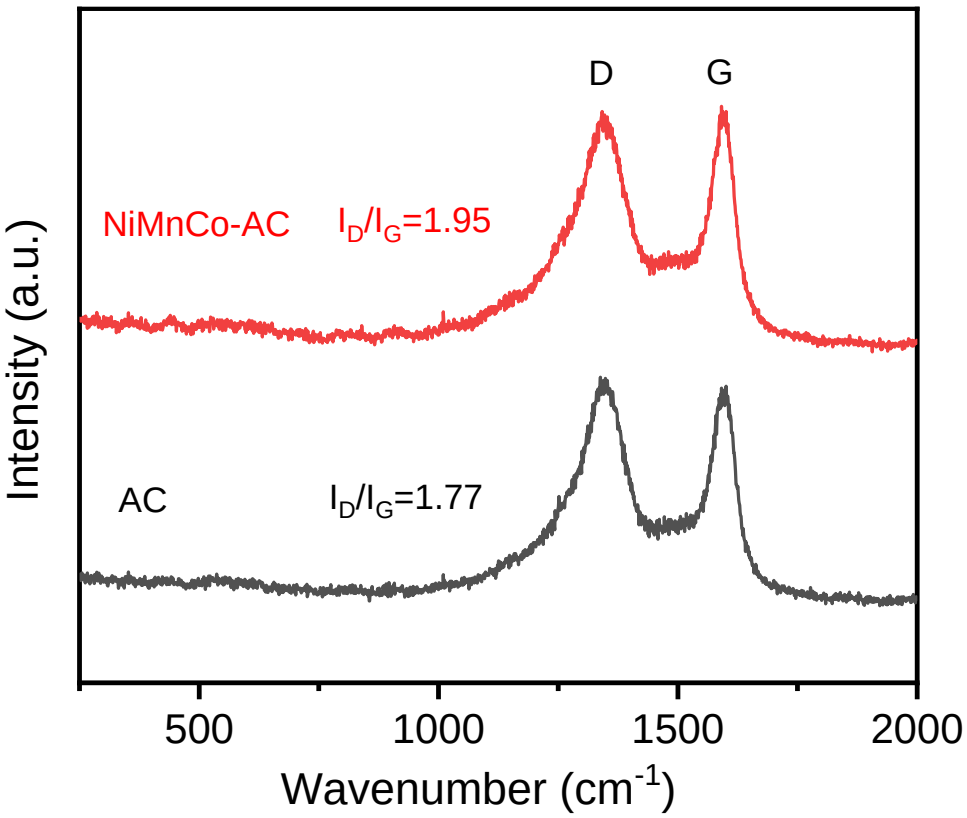

Figure S4 Raman curves of the NiMnCo-AC and AC samples.

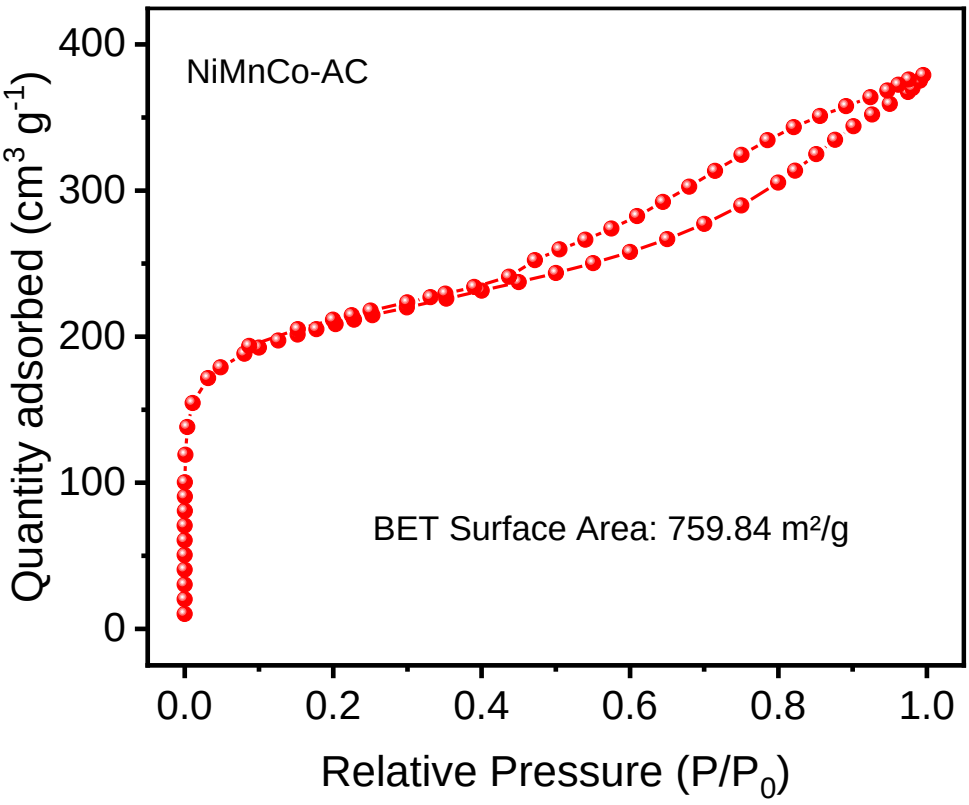

Figure S5 Nitrogen adsorption-desorption isotherms of the NiMnCo-AC catalyst.

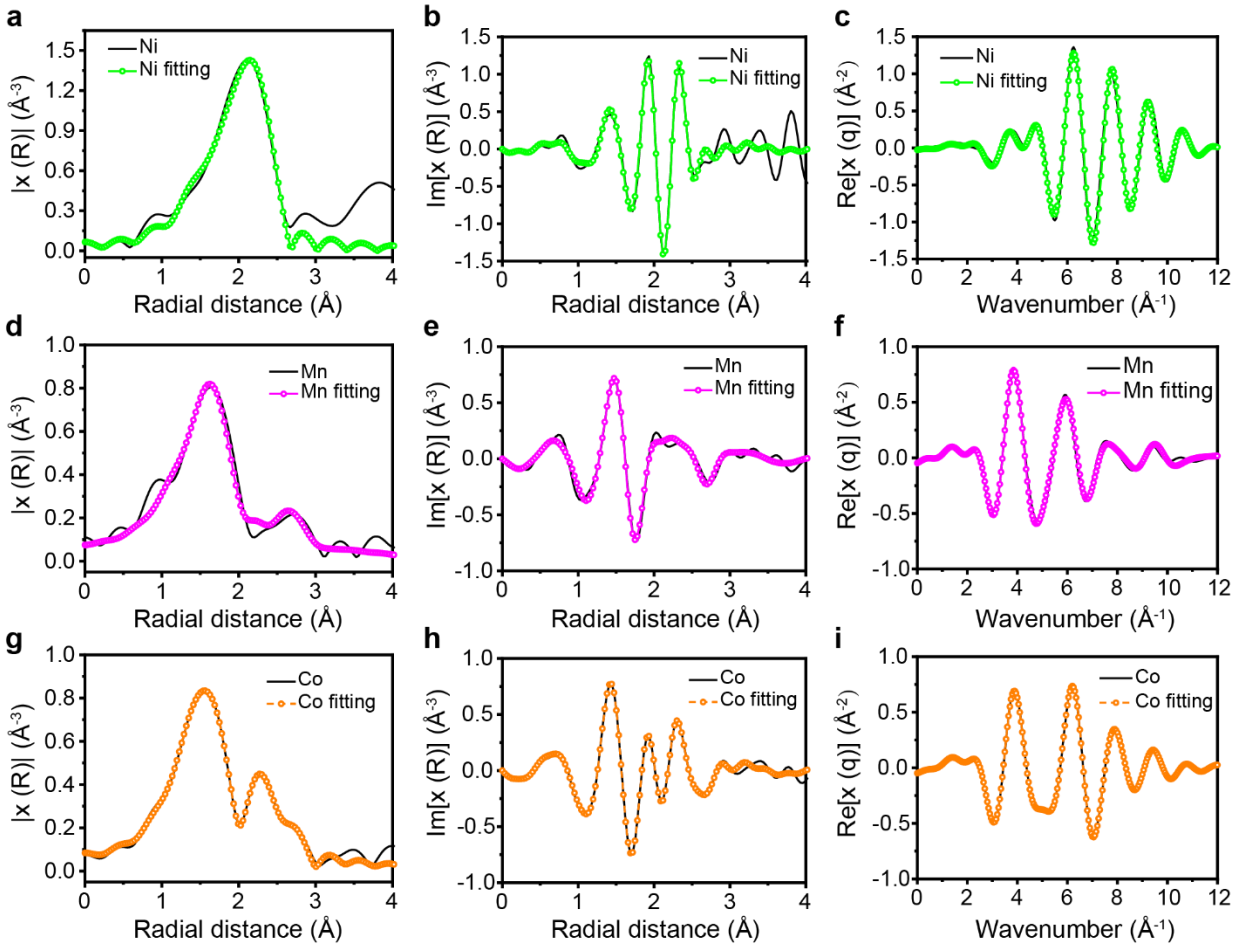

Figure S6 EXAFS spectra fitting results of the NiMnCo-AC. **a**, Ni K edge k^2-weighted R space EXAFS fitting results. **b**, Ni K edge k^2-weighted FT imaginary fitting results. **c**, Ni K edge k^2-weighted q space fitting results. **d**, Mn K edge k^2-weighted R space EXAFS fitting results. **e**, Mn K edge k^2-weighted FT imaginary fitting results. **f**, Mn K edge k^2-weighted q space fitting results. **g**, Co K edge k^2-weighted R space EXAFS fitting results. **h**, Co K edge k^2-weighted FT imaginary fitting results. **i**, Co K edge k^2-weighted q space fitting results.

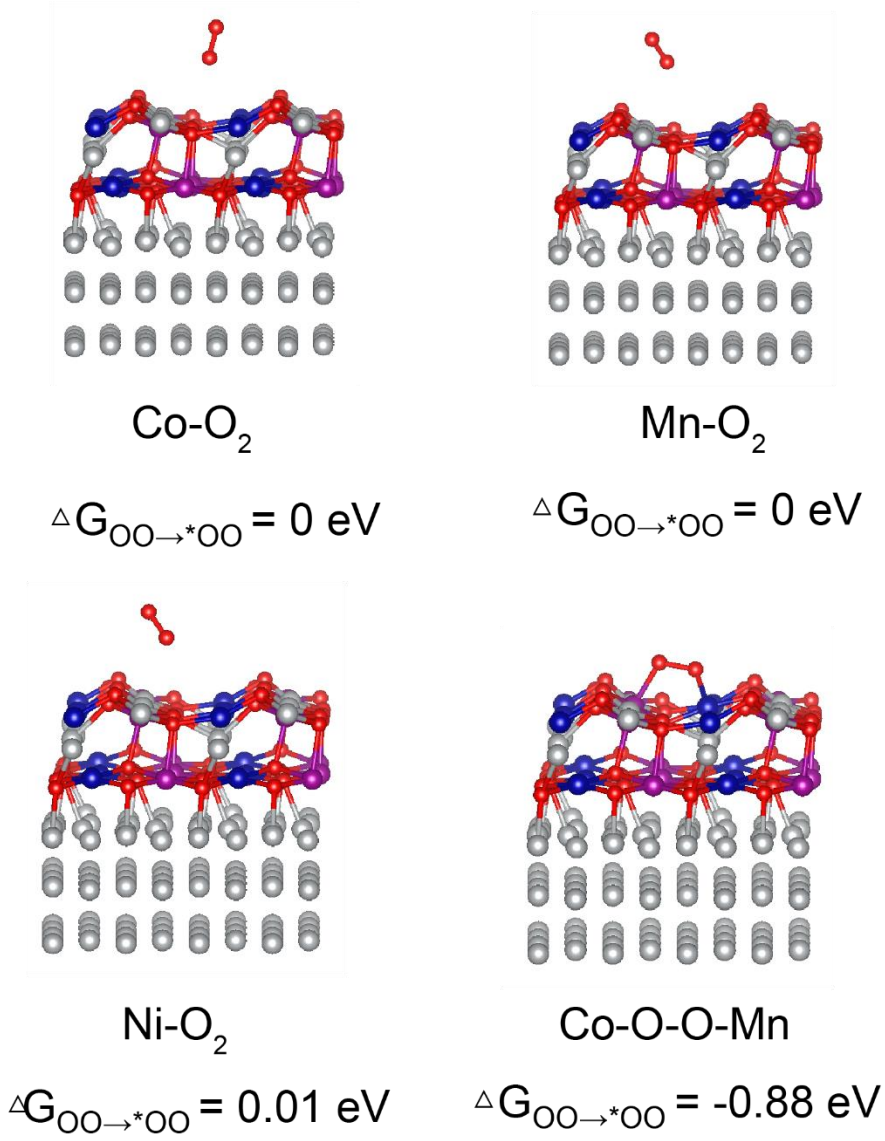

Figure S7 All the adsorbed models of O_2 on Ni(111)@$NiMnCoO_4$(110) and the corresponding adsorption Gibbs free energy.

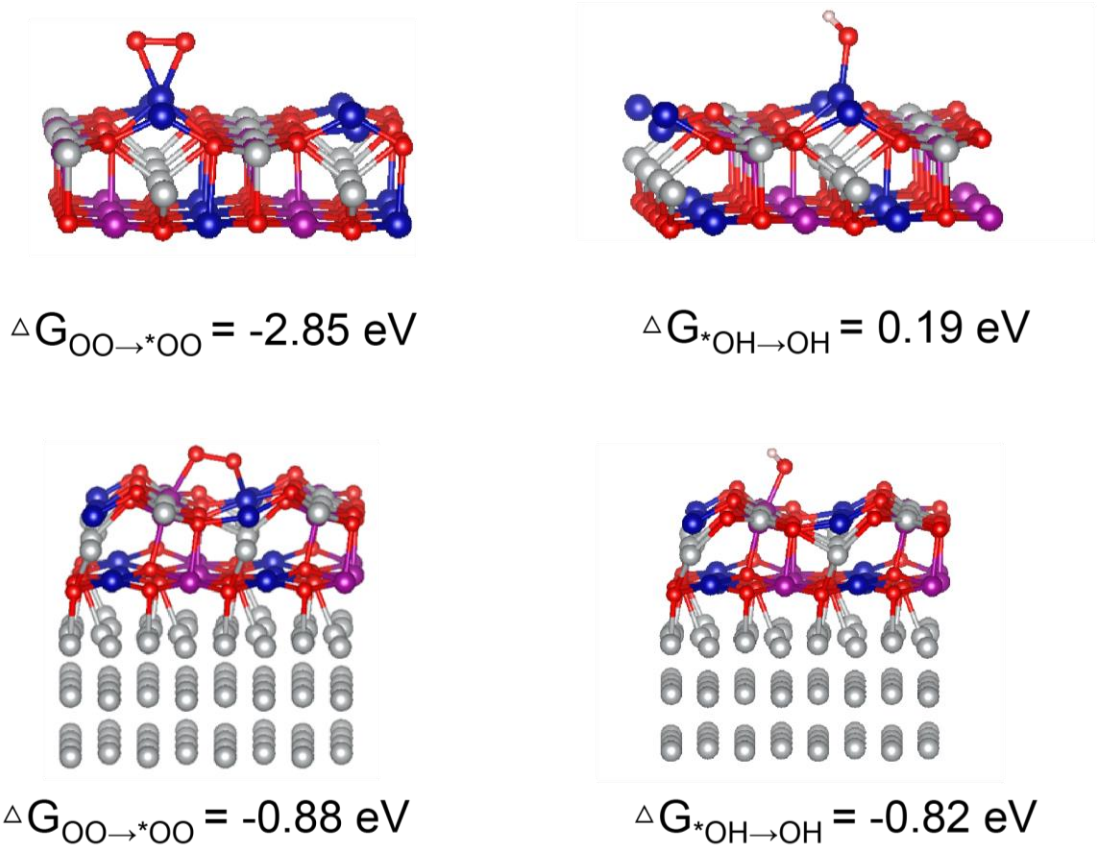

Figure S8 The adsorbed models of O_2/OH on Ni(111)@$NiMnCoO_4$(110) and $NiMnCoO_4$(110), and the corresponding adsorption Gibbs free energy.

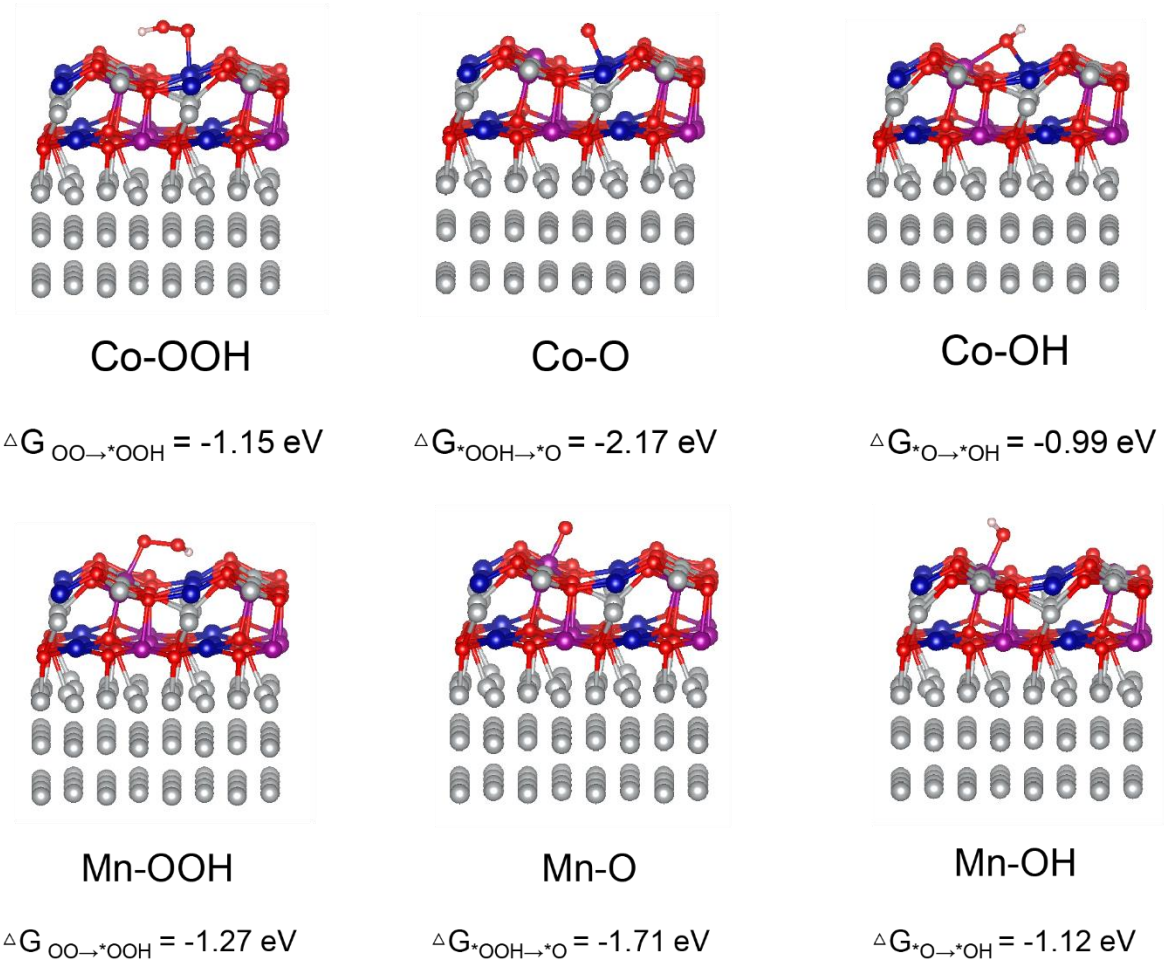

Figure S9 Adsorbed structures of intermediates on Ni(111)@$NiMnCoO_4$(110) and the corresponding Gibbs free energy.

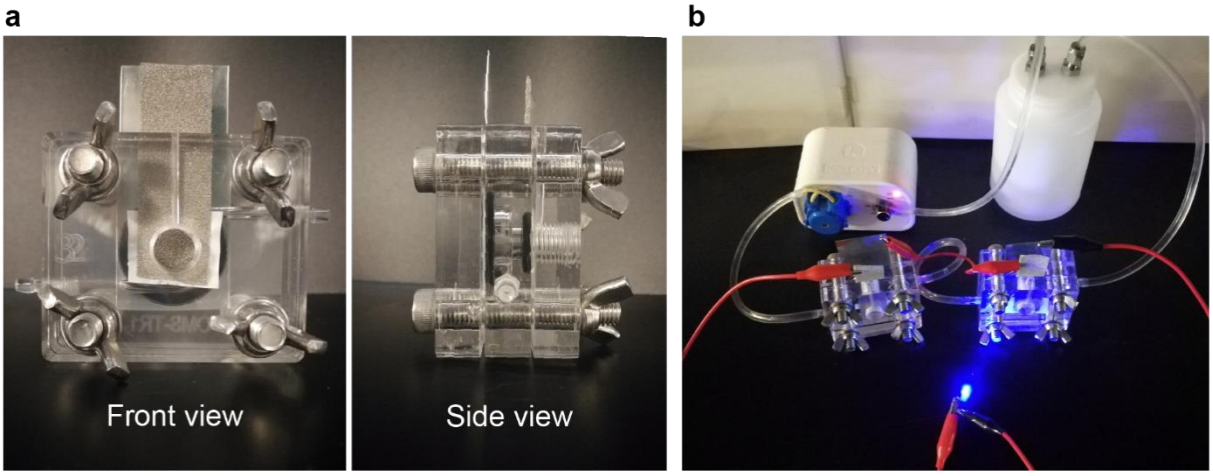

Figure S10 a, Front view and side view of primary zinc-air battery. **b**, A blue LED can be lighted up by two ZABs in series developed by NiMnCo-AC catalyst as the air cathode.

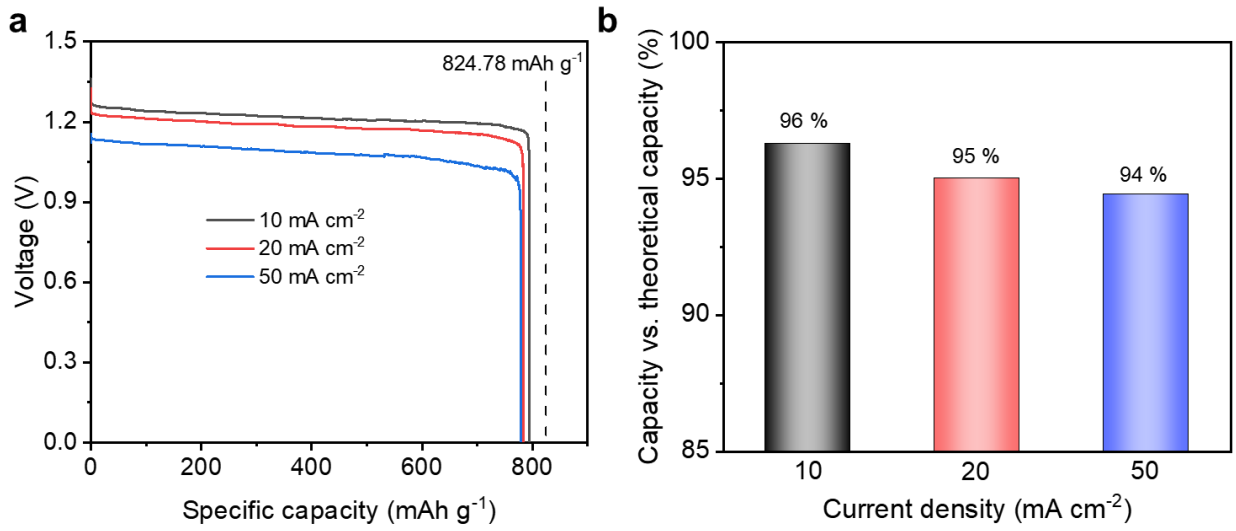

Figure S11 a, Discharge curves of the ZAB with NiMnCo-AC catalyst at the current density of 10, 20, and 50 mA cm^{-2}. **b**, Discharge percentages of the ZAB with NiMnCo-AC catalyst versus the theoretical capacity of zinc-air battery at various current densities.

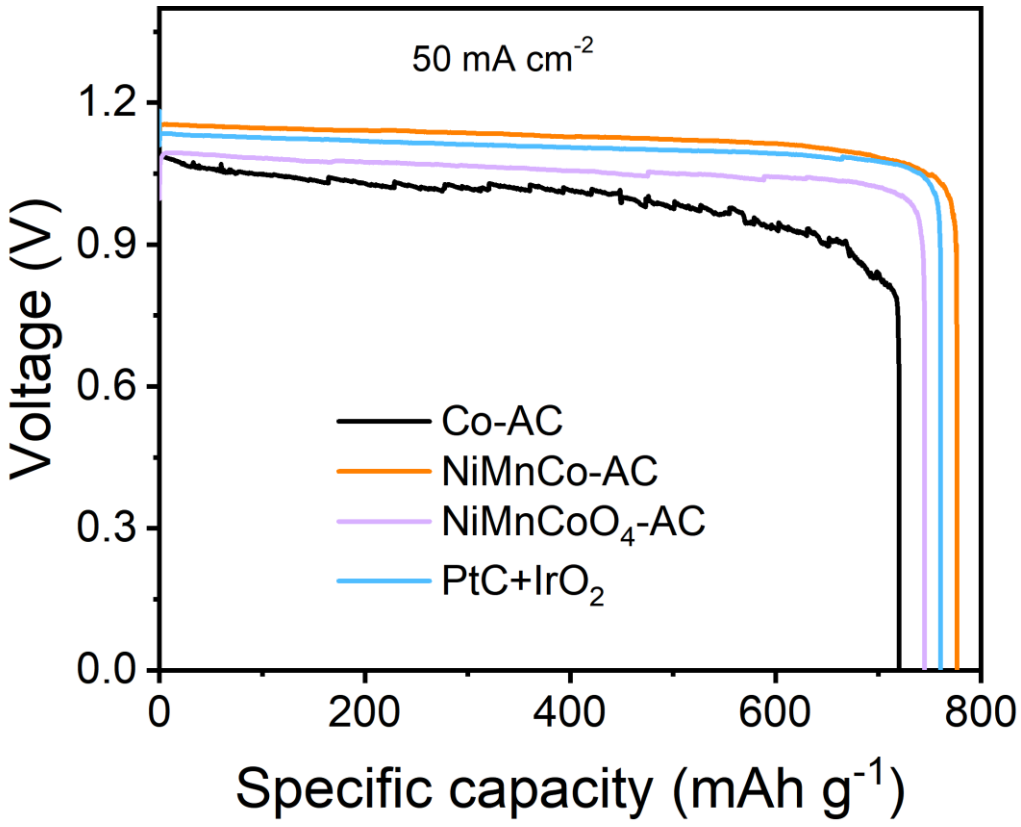

Figure S12 The comparison of discharge performance of ZABs with NiMnCo-AC, Co-AC, $NiMnCoO_4$-AC, and PtC/IrO_2 at the current density of 50 mA cm^{-2}.

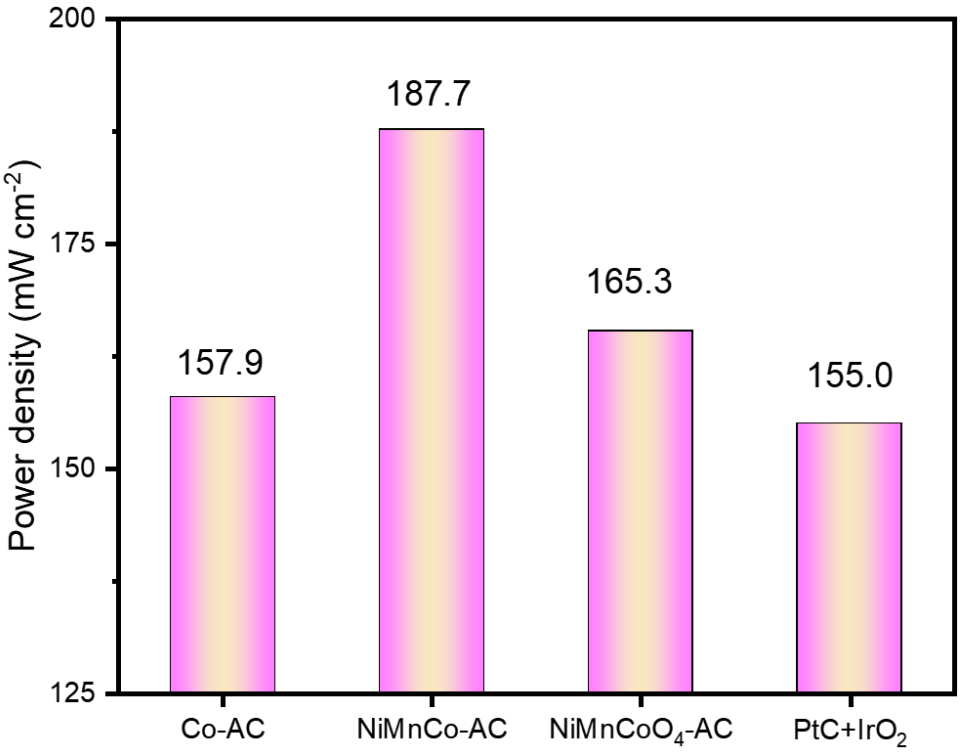

Figure S13 Comparison of the power densities of ZABs with Co-AC, NiMnCo-AC, $NiMnCoO_4$-AC, and PtC/IrO_2 catalysts. The NiMnCo-AC exhibits a highest power density of 187.698 wh cm^{-2}, which is 32.68 wh cm^{-2} higher than the commercial PtC/IrO_2.

Table S1 Curve fit parameters for Ni K-edge EXAFS for NiMnCo-AC catalyst

Scattering path	Distance (Å)	C.N.[a]	σ^2 (Å^2)	ΔE_0 (eV)	R-factor
Ni-Ni	2.50	4.9	0.007	-2.8	0.017
Ni-O	2.03	2.8	0.006	-2.8	

[a] C.N. is the coordination number. Fitting was conducted by k^2-weighted R space EXAFS spectra with the k range of 3.0-11.0 Å^{-1} and the R range of 1.0-3.0 Å.

Table S2 Curve fit parameters for Mn K-edge EXAFS for NiMnCo-AC catalyst

Scattering path	Distance (Å)	C.N.[a]	σ^2 (Å^2)	ΔE_0 (eV)	R-factor
Mn-O	2.12	4.5	0.010	-3.6	
Mn-M (Ni, Co, Mn)	2.50	0.2	0.019	-3.6	0.016
Mn-O-M (Ni, Co, Mn)	3.09	0.8	0.013	-3.6	

[a] C.N. is the coordination number. Fitting was conducted by k^2-weighted R space EXAFS spectra with the *k* range of 3.0-11.0 Å^{-1} and the R range of 1.0-3.0 Å.

Table S3 Curve fit parameters for Co K-edge EXAFS for NiMnCo-AC catalyst

Scattering path	Distance (Å)	C.N.[a]	σ^2 (Å^2)	ΔE_0 (eV)	R-factor
Co-O	2.03	5.1	0.009	-1.301	
Co-M (Ni, Co, Mn)	2.49	0.6	0.003	-1.301	0.001
Co-O-M (Ni, Co, Mn)	3.02	1.6	0.013	-1.301	

[a] C.N. is the coordination number. Fitting was conducted by k^2-weighted R space EXAFS spectra with the k range of 3.0-11.0 Å^{-1} and the R range of 1.0-3.0 Å.

Table S4 Estimated crystal size of Ni by the Debye-Scherrer method

Selected crystal phase	Ni (111)
K (Scherrer constant)	0.89
B (FWHM)	1.96
2θ (Position of diffraction peak)	44.5°
γ (Wavelength)	1.54 (Å)
D (Estimated size)	7.6 (nm)